ISSN:1687-1006

The Egyptian International Journal of Engineering Sciences and Technology

Vol. 19 No. 2 (2016-Special Issue) 282–296

http://www.eijest.zu.edu.eg

A Comparative Study of Supercavitation Phenomena on Different Projectiles Shapes in Transient Flow by CFD

Mohsen Y. Mansour[1]*, Mohamed H. Mansour[2], Nabil H. Mostafa[3] and Magdy Abu Rayan[2]

[1]*Aeronautical Eng., Mansoura University, Egypt*
[2]*Mechanical Power Department, Mansoura University, Egypt*
[3]*Mechanical Power Department, Zagazig University, Zagazig, P.O. 44519, Egypt*

ARTICLE INFO

Article history:
Received 13 May 2016
Received in revised form
7 June 2016
Accepted 14 June 2016
Available online 1 July 2014

Keywords:
Supercavitation;
Structured grid;
Unstructured grid;
ESI-CFD;
Hydrofoil;
Projectile;
Shape optimization.

ABSTRACT

Body shape of high-speed underwater vehicles has a great effect on the Supercavitation behaviour. The transient flow around either partially cavitating or supercavitating body affects the trajectory of high-speed underwater vehicles. Commercial code (ESI-CFD ACE+, V 2010) was used to simulate the supercavitation around two different shapes of a projectile with their noses of hemispherical shape and telescopic shape. Also, conical and blunt projectile shapes were considered. Also, a comparison between two different designs of grid was performed numerically. Grid designs were structured and unstructured grids. Navier-Stokes equations were used as governing equations for simulating supercavitation. Cavity shape was determined over projectile body and around wake. Also, two-dimensional flow field around the cavitating body was determined. Projectile body has a diameter about 0.4 times its length (0.4L). In the case of the Blunt end there is a strong wake effect. The ESI-CFD code (2010) is valid for observing the supercavitation phenomena. Unstructured grid is more accurate than structured one in simulating supercavitation.

1. Introduction

High-speed underwater vehicles have many advantages and disadvantages. So, many researchers simulate is behaviour and try to control is trajectory. Mostafa et al. (2001) study experimentally the flow around a hemisphere cylinder by shooting a projectile and employing Particle Image Velocimetry (PIV) to measure the velocity field. A doublet is generated between the projectile nose and its rear end. At high speeds, a vortex ring is situated over the bubble boundary.

The flow around either partially cavitating or supercavitating hydrofoils are treated by Kinnas et al. (1994) with a viscous/ inviscid interactive method. Owis and Nayfeh (2003) compute the compressible Multiphase Flow Over the cavitating high-speed torpedo. The cavitating flow over hemispherical and conical bodies indicate that the preconditioned system of equations converges rapidly to the required solution at very low speeds.

* Corresponding author. Tel.: +201009387559.
E-mail address: mohsen_mansour@hotmail.com.

To improve the understanding of the unsteady behaviour of supercavitating flows, Mostafa (2005) used a three-dimensional Navier-Stokes code to model the two-phase flow field around a hemisphere cylinder. The governing equations are discretized on a structured grid using an upwind difference scheme.

Supercavitating vehicles exploit supercavitation as a means to reduce drag and achieve an extremely high underwater speed. Supercavitation is achieved when a body moves through water at sufficient speed, so that the fluid pressure drops to the water vapor pressure. In supercavitating flows, a low-density gaseous cavity entirely envelops the vehicle and the skin drag of the vehicle is almost negligible. Hence, the vehicle can move at extremely high speed in a two-phase medium, Ahn (2007). So, A supercavitating torpedo is a complex high speed undersea weapon that is exposed to extreme operating conditions due to the weapon's speed. Alyanak et al. (2006) formulates an optimize this problem to determines the general shape of the torpedo in order to satisfy the required performance criteria function of speed. Kamada (2005).

The object of this work is to study the transit flow around either partially cavitating or supercavitating body affecting the high-speed underwater vehicles, which have different body shapes and cavitation numbers. Calculation will use structured grids and un-structured grids Structure

Nomenclature

C_e , C_c	phase change rate coefficients	
D	projectile diameter	m
f	vapor mass fraction	
L	Projectile length	m
κ	turbulence kinetic energy	m^2/s^2
P	fluid static pressure	N/m^2
p_{sat}	saturation pressure	N/m^2
P'_{turb}	magnitude of pressure fluctuations	N/m^2
P_t	total pressure	N/m^2
R	universal gas constant	Nm/Kg.k
R	the rate of phase change	
R_{en}	Renold number	
T	fluid temperature	K
Δt	physical time step	second
u,v,w	velocity in x, y, w respectively	m/s
$\vec{V}$	velocity vector	
V_{ch}	characteristic velocity $V_{ch}=\sqrt{\kappa}$	
W	molecular weight	kg/kg-mol

Greek letters

α	vapor volume fraction	
σ	cavitation number $((p_\infty - p_v)/(1/2\rho_l u^2))$	N/m
ρ	the mixture density	Kg/m^3
Γ	effective exchange coefficient	

Suffixes

c	bubble reduction and collapse
e	bubble generation and expansion
gas, G	gas phases
L	liquid phases
V	vapor phases

Theory Background

The calculation of cavitation phenomena in this paper is based on solving Navier-Stokes equations through cavitation module of ESI - CFD 2010 and K-ε turbulence model. A numerical model previously developed by ESI-CFD to solve (Navier- Stokes) equations (Sighal, 1999).

As we know in cavitational flow as 2D flow, the mixture mass density (ρ) is function of vapour mass fraction (f), water density and vapour density. The ρ - f relationship is:

$$\frac{1}{\rho} \equiv \frac{f}{\rho_v} + \frac{1-f}{\rho_1} \tag{1}$$

The previous equation can be written by using vapour volume fraction. Therefore, it is deduced from f as follows:

$$\alpha = f\frac{\rho}{\rho_v} \tag{2}$$

The transport equation for vapor is written as follows:

$$\frac{\partial}{\partial t}(\rho f) + V \bullet (\rho \vec{V} f) = V \bullet (\Gamma \nabla f) + R_e - R_c \tag{3}$$

The expressions of R_e and R_c have been derived from the reduced form of the Rayleigh-Plesset equation (Hammitt, 1980), which describes the dynamics of single bubble in an infinite liquid domain. The expressions for R_e and R_c are:

$$R_e = C_e \frac{V_{ch}}{\sigma} \rho_l \rho_v \sqrt{\frac{2}{3}\frac{p_{sat} - p}{\rho_l}} (1-f) \tag{4}$$

$$R_c = C_c \frac{V_{ch}}{\sigma} \rho_l \rho_v \sqrt{\frac{2}{3}\frac{p - p_{sat}}{\rho_l}} f \tag{5}$$

As we know that cavitation occurs in flow areas where flow velocity is very high or flow pressure is very low and approach to the water vapour pressure. The magnitude of pressure fluctuations is estimated by using the following empirical correlation (Hinze, 1975):

$$P'_{turb} = 0.39\,\rho\,k \quad (6)$$

The phase-change threshold pressure value is as:

$$p_v = p_{sat} + 0.5 p'_{turb} \quad (7)$$

In this model due to low flow pressure, we put the dissolved (non condensable) gases in cavitation calculations. However, the corresponding density (and hence volume fraction) varies significantly with local pressure. The perfect gas law is used to account for the expansion (or compressibility) of gas; i.e.,

$$\rho_{gas} = \frac{WP}{RT} \quad (8)$$

The calculation of mixture density (equation 1) is modified as:

$$\frac{1}{\rho} = \frac{f_v}{\rho_v} + \frac{f_g}{\rho_g} + \frac{1 - f_v - f_g}{\rho_l} \quad (9)$$

We have the following expression for the volume fractions of vapor (α_v) and gas (α_g):

$$\alpha_v = f_v \frac{\rho}{\rho_v} \quad (10)$$

$$\alpha_g = f_g \frac{\rho}{\rho_g} \quad (11)$$

and,

$$\alpha_l = 1 - \alpha_v - \alpha_g \quad (12)$$

The combined volume fraction of vapor and gas (i.e., $\alpha_v + \alpha_g$) is referred to as the Void Fraction (α). In practical applications, for qualitative assessment of the extent and location of cavitation, contour maps of void fraction (α) are important.

Results and Discussion

In present research, supercavitation around projectile is simulated for two different projectile shapes. Hemisphere projectile has a hemispherical shape from both sides. Telescopic projectile is a telescopic shape at nose and flat shape at tail. Both shapes are modelled by use two different grid designs, structured and unstructured. The used grids are structured mesh and unstructured mesh grids. The projectile is projected horizontally by speed 60 m/s in water. All present figures are according the projectile is moved from right to left except figure 21 which depend on moving the projectile from left to right.

Also, the projectile dimensions are related to D/L= 0.4. Comparison between two grids is performed. Table 1 shows the data of each grid. The table illustrates the number of cells, number of nodes, number of zones, and the time consumed to solve one time-step for each case.

Table 1: Comparison between the two grids in mesh specifications for both projectiles.

	Hemisphere projectile		Telescopic projectile	
	Structured	Unstructured	Structured	Unstructured
Cells	25,043	28,768	28,089	26,222
nodes	25,440	14,615	28,990	13,337
zones	3	1	6	1
time (min)	0.5	0.1	2.5	2

The used computer for simulation the present study for both cases is a workstation with specifications:

Processor: double Intel Xeon CPU E5-2620 v2 @ 2.10 GHz
Memory: 16 GB

The transient cavitation flow analysis is computed for cavitation number of 0.0555. Used time-step interval is $1\text{x}10^{-5}$ sec.

3.1 hemisphere projectile

Hemisphere projectile is hemispherical projectile on two sides. The structured grid for this projectile is used as shown in figure 1a. The structure grids are divided into three zones.

Unstructured grid of the projectile, shown in figure 1b, is performed in one zone domain. The grids are clustered near the body to solve the boundary layer. The physical time step is taken to be $1\text{x}10^{-5}$ second for the unsteady flow computations in order to resolve accurately the transients of the supercavitating flow.

Figures 5 and 6 display the iso-density contours for cavitating flow over both grids of hemispherical body in a time sequence of the bubble shape. This hemisphere projectile has half spheres from both sides at diameter 0.4 L. The cavitation number is σ =0.0555 at speed of u= 60 m/s. It is demonstrated that the cavity formation has five stages. First, a cavity starts to grow at the wake of the body only due to its low pressure. At the second stage, another cavity grows beside the nose while the cavity at the body wake continues to grow. The cavity beside the nose grows enough to affect the pressure at the body wake, so, the cavity at the body wake starts to collapse at the third stage. In the fourth stage, the cavity beside the nose grows enough to merge with the cavity at the body wake. Finally, that cavity starts to have a fluctuation around the final shape.

Figures 13 and 14 represent the distribution of void fraction, total pressure, static pressure and velocity magnitude. The void fraction contour is approximately similar to the iso-density contours as well as the iso-total pressure contours. There is a reverse flow in the horizontal velocity component at the cavities region near to the body and in the body wake. The maximum vertical velocity component is concentrated around the front nose. In this case, the maximum turbulence kinetic energy is around the front nose similar to the iso-pressure contour.

Figures show observation which is finding a vortex in the nose area by using unstructured grid of telescopic projectile. This vortex is in agreement with actual (experimental) case of Mostafa et al. (2001). The results by structured grid did not show this vortex.

3.2 telescopic projectile

Telescopic projectile is telescopic-nose projectile and flat at tail. The structured grid for this projectile is used as shown in figure 2a. Structured mesh is refined but by dividing the domain to 3 zones.

In present case of structured grid telescopic projectile is used as shown in figure 2a. The structure grids are divided into three zones.

Unstructured grid of the projectile, shown in figure 2b, is performed in one zone domain. The grids are clustered near the body to solve the boundary layer. The physical time step is taken to be $1x10^{-5}$ second for the unsteady flow computations in order to resolve accurately the transients of the supercavitating flow.

Figures 7 and 8 display the iso-density contours for cavitating flow over both grids of hemispherical body in a time sequence of the bubble shape. This hemisphere projectile has half spheres from both sides at diameter 0.4 L. The cavitation number is σ =0.0555 at speed of u= 60 m/s. It is demonstrated that the cavity formation has five stages. First, a cavity starts to grow at the wake of the body only due to its low pressure. At the second stage, another cavity grows beside the nose while the cavity at the body wake continues to grow. The cavity beside the nose grows enough to affect the pressure at the body wake, so, the cavity at the body wake starts to collapse at the third stage. In the fourth stage, the cavity beside the nose grows enough to merge with the cavity at the body wake forming a large one. Finally, that cavity starts to have a fluctuation around the final shape.

Figures 15 and 16 represent the distribution of void fraction, total pressure, pressure and velocity magnitude. Also, void fraction contour is approximately similar to the iso-density contours as well as the iso-total pressure contours. There is a reverse flow in the horizontal velocity component at the cavities region near to the body and in the body wake. The maximum vertical velocity component is concentrated around the front nose. In this case, the maximum turbulence kinetic energy is around the front nose similar to the iso-pressure contour.

3.3 blunt projectile

Blunt projectile is flat-nose projectile and flat at tail. The structured grid for this projectile is used as shown in figure 3a. Structured mesh is refined but by dividing the domain to 3 zones.

In present case of structured grid blunt projectile is used as shown in figure 3a. The structure grids are divided into three zones.

Unstructured grid of the projectile, shown in figure 3b, is performed in one zone domain. The grids are clustered near the body to solve the boundary layer. The physical time step is taken to be $1x10^{-5}$ second for the unsteady flow computations in order to resolve accurately the transients of the supercavitating flow.

Figures 9 and 10 display the iso-density contours for cavitating flow over both grids of blunt body in a time sequence of the bubble shape. This hemisphere projectile has half spheres from both sides at diameter 0.4 L. The cavitation number is σ =0.0555 at speed of u= 60 m/s. It is demonstrated that the cavity formation has five stages. First, a cavity starts to grow at the wake of the body only due to its low pressure. At the second stage, another cavity grows beside the nose while the cavity at the body wake continues to grow. The cavity beside the nose grows enough to affect the pressure at the body wake, so, the cavity at the body wake starts to collapse at the third stage. In the fourth stage, the cavity beside the nose grows enough to merge with the cavity at the body wake forming a large one. Finally, that cavity starts to have a fluctuation around the final shape.

Figures 17 and 18 represent the distribution of void fraction, total pressure, pressure and velocity magnitude. Also, void fraction contour is approximately similar to the iso-density contours as well as the iso-total pressure contours. There is a reverse flow in the horizontal velocity component at the cavities region near to the body and in the body wake. The maximum vertical velocity component is concentrated around the front nose. In this case, the maximum turbulence kinetic energy is around the front nose similar to the iso-pressure contour.

3.4 conical projectiles

Conical projectile is conical-nose projectile and flat at tail. The structured grid for this projectile is used as shown in figure 4a. Structured mesh is refined but by dividing the domain to 3 zones.

In present case of structured grid conical projectile is used as shown in figure 4a. The structure grids are divided into three zones.

Unstructured grid of the projectile, shown in figure 4b, is performed in one zone domain. The grids are clustered near the body to solve the boundary layer. The physical time step is taken to be $1x10^{-5}$ second for the unsteady flow computations in order to resolve accurately the transients of the supercavitating flow.

Figures 11 and 12 display the iso-density contours for cavitating flow over both grids of conical body in a time sequence of the bubble shape. This conical projectile has half spheres from both sides at diameter 0.4 L. The cavitation number is σ =0.0555 at speed of u= 60 m/s. It is demonstrated that the cavity formation has five stages. First, a cavity starts to grow at the wake of the body only due to its low pressure. At the second stage, another cavity grows beside the nose while the cavity at the body wake continues to grow. The cavity beside the nose grows enough to affect the pressure at the body wake, so, the cavity at the body wake starts to collapse at the third stage. In the fourth stage, the cavity beside the nose grows enough to merge with the cavity at the body wake forming a large one. Finally, that cavity starts to have a fluctuation around the final shape.

Figures 19 and 20 represent the distribution of void fraction, total pressure, pressure and velocity magnitude. Also, void fraction contour is approximately similar to the iso-density contours as well as the iso-total pressure contours. There is a reverse flow in the horizontal velocity component at the cavities region near to the body and in the body wake. The maximum vertical velocity component is concentrated around the front nose. In this case, the maximum turbulence kinetic energy is around the front nose similar to the iso-pressure contour.

3.5 comparisons and observations

Mostafa et al. (2001) illustrate the formation of cavity during supercavitation around a projectile. Figure 21 shows their experimental results that confirmed existence of two types of vortices. First type is at projectile nose. Second one is at projectile tail.

Figures show a new note is observed which existence of a vortex in the nose area is by using unstructured grid of telescopic projectile. This vortex is in agreement with actual (experimental) case of Mostafa et al. (2001) as in figure 21. The results by structured grid did not show this vortex.

4 Summary and Conclusions

The unsteady flow around either partially cavitating or supercavitating high-speed underwater vehicles is simulated. Also, the accuracy of results is affected by grid design.

Cavity formation five stages goes through First, a cavity starts to grow at the wake of the body only due its low pressure. At the second stage, another cavity grows beside the nose while the cavity at the body wake continues to grow. The cavity beside the nose grows enough to affect the pressure at the body wake, so, the cavity at the body wake starts to collapse at the third stage. In the fourth stage, the cavity beside the nose grows enough to merge with the cavity at the body wake forming a large one. Finally, that cavity starts to fluctuate around the final shape.

There is a reverse flow in the horizontal velocity component at the cavities region near to the body and in the body wake. The maximum vertical velocity component is concentrated around the front nose.

New note is observed which is finding a vortex in the nose area by using unstructured grid of telescopic projectile. This vortex is in agreement with actual (experimental) case of Mostafa et al. (2001). The results by structured grid did not show this vortex.

Using unstructured grid is better than structured one for water-flow simulation of supercavitation for a hemispherical projectile.

Using ESI-CFD commercial code is valid for simulating supercavitation around projectiles in water.

a) structured mesh b) unstructured mesh

Fig. (1) Grid over hemisphere projectile.

a) structured mesh b) unstructured mesh

Fig. (2) Grid over telescopic projectile.

a) structured mesh b) unstructured mesh

Fig. (3) Grid over blunt projectile.

a) structured mesh b) unstructured mesh

Fig. (4) Grid over conical projectile.

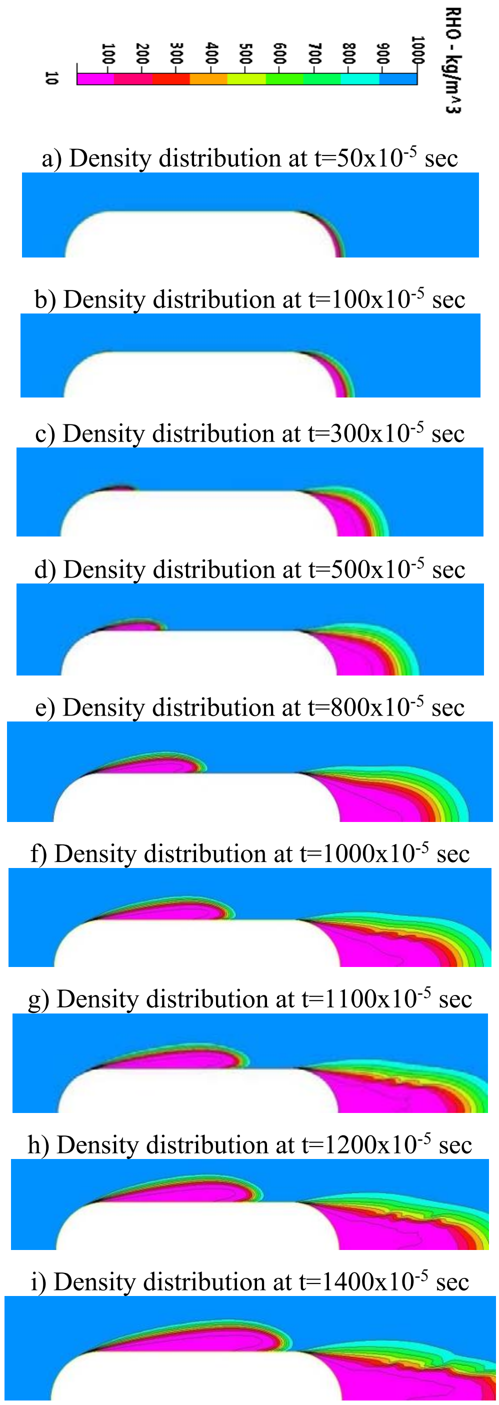

Fig. (5) Supercavitating cavities formation upon hemisphere projectile at speed 60 m/s, using structured mesh domain.

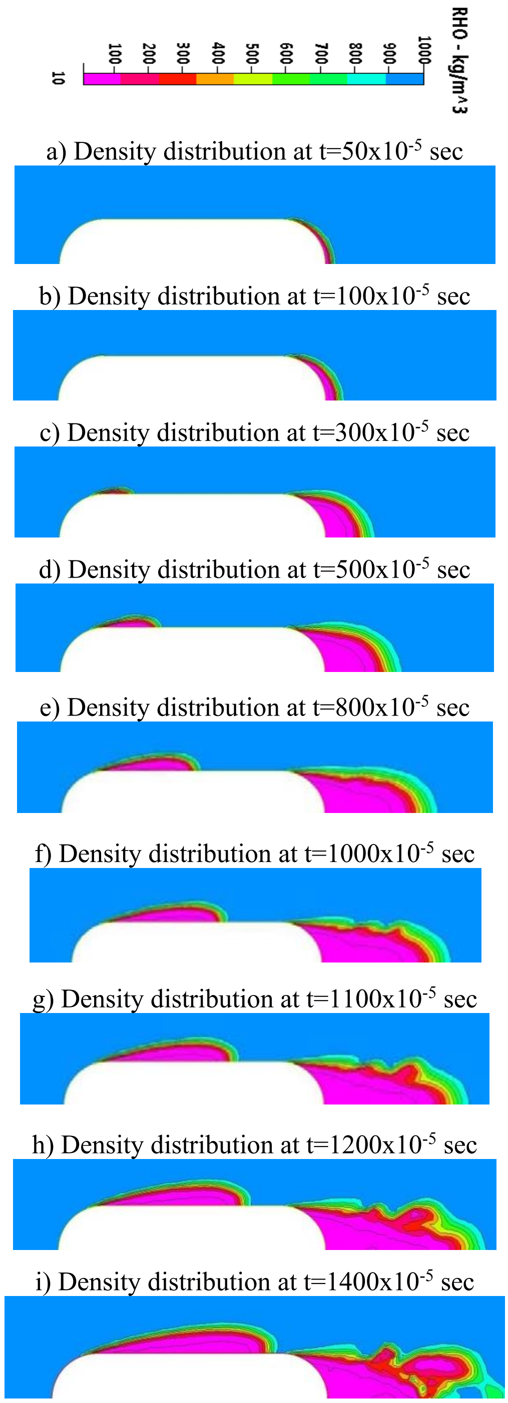

Fig. (6) Supercavitating cavities formation upon hemisphere projectile at speed 60 m/s, using unstructured mesh domain.

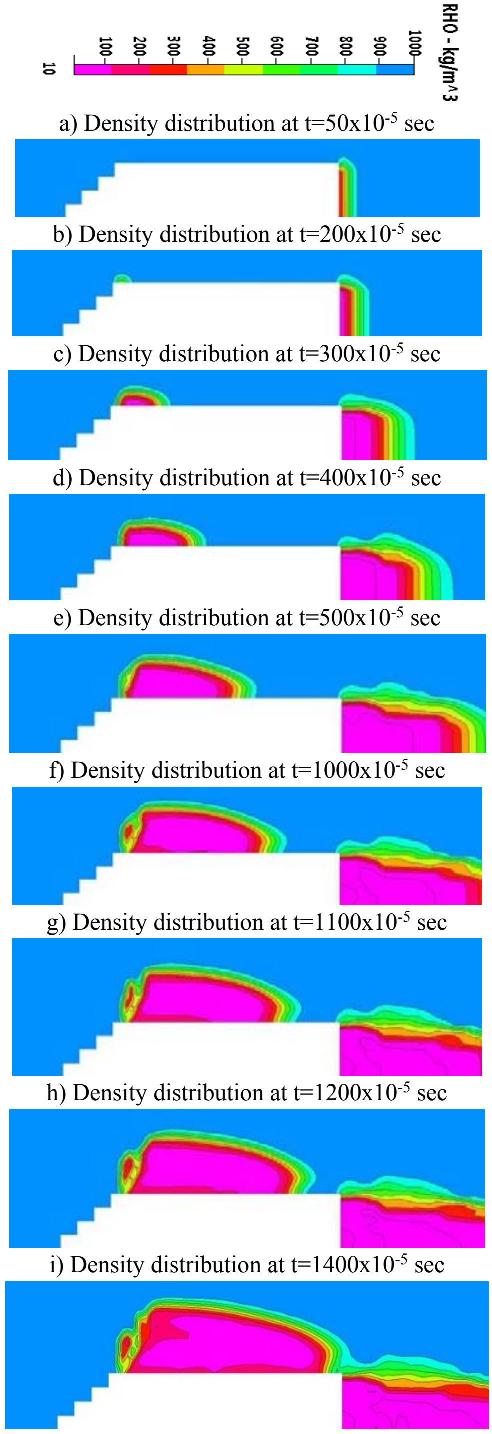

Fig. (7) Supercavitating cavities formation upon telescopic projectile at speed 60 m/s, using structured mesh domain.

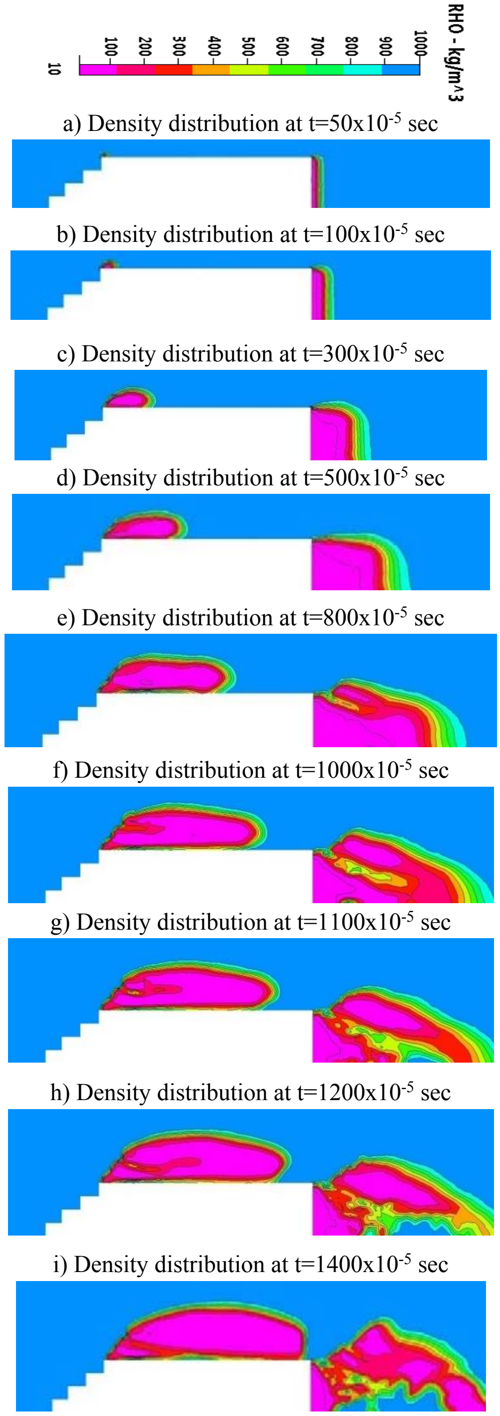

Fig. (8) Supercavitating cavities formation upon telescopic projectile at speed 60 m/s, using unstructured mesh domain.

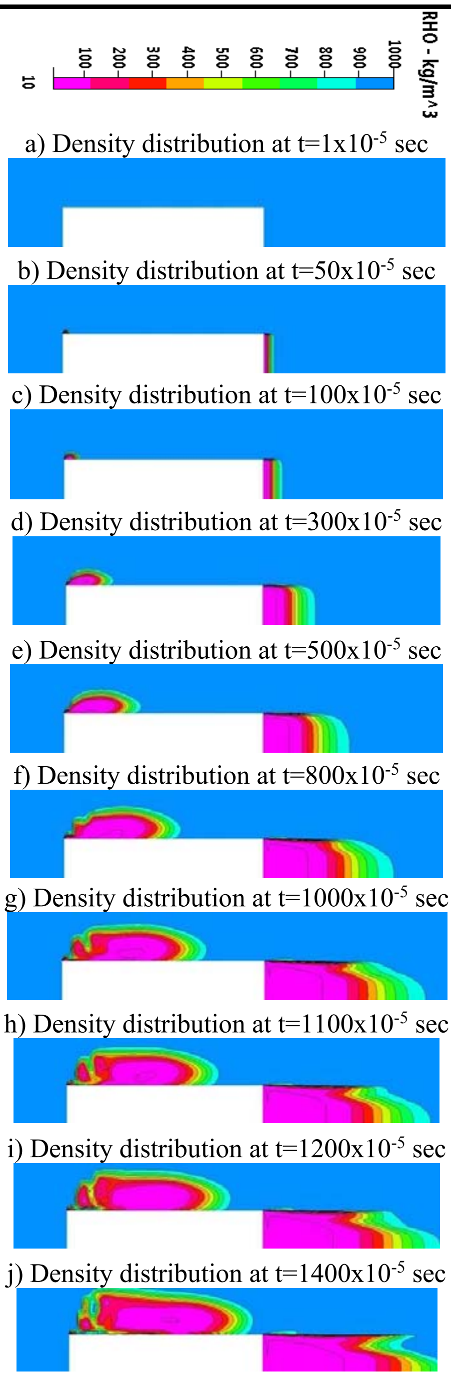

Fig. (9) Supercavitating cavities formation upon blunt projectile at speed 60 m/s, using structured mesh domain.

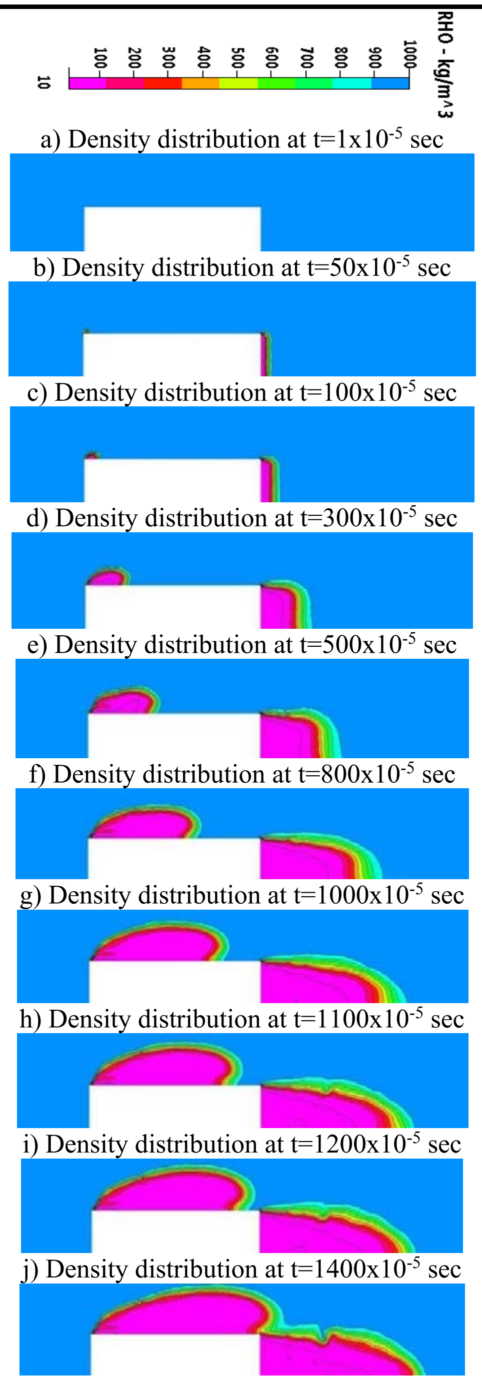

Fig. (10) Supercavitating cavities formation upon blunt projectile at speed 60 m/s, using unstructured mesh domain.

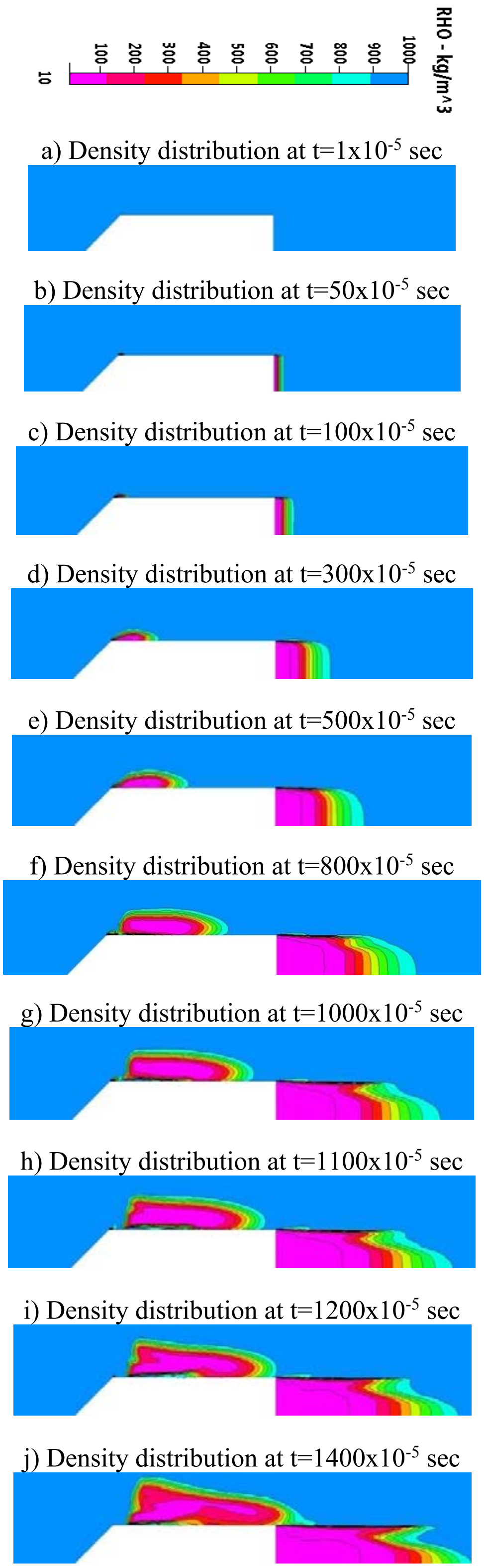

Fig. (11) Supercavitating cavities formation upon conical projectile at speed 60 m/s, using structured mesh domain.

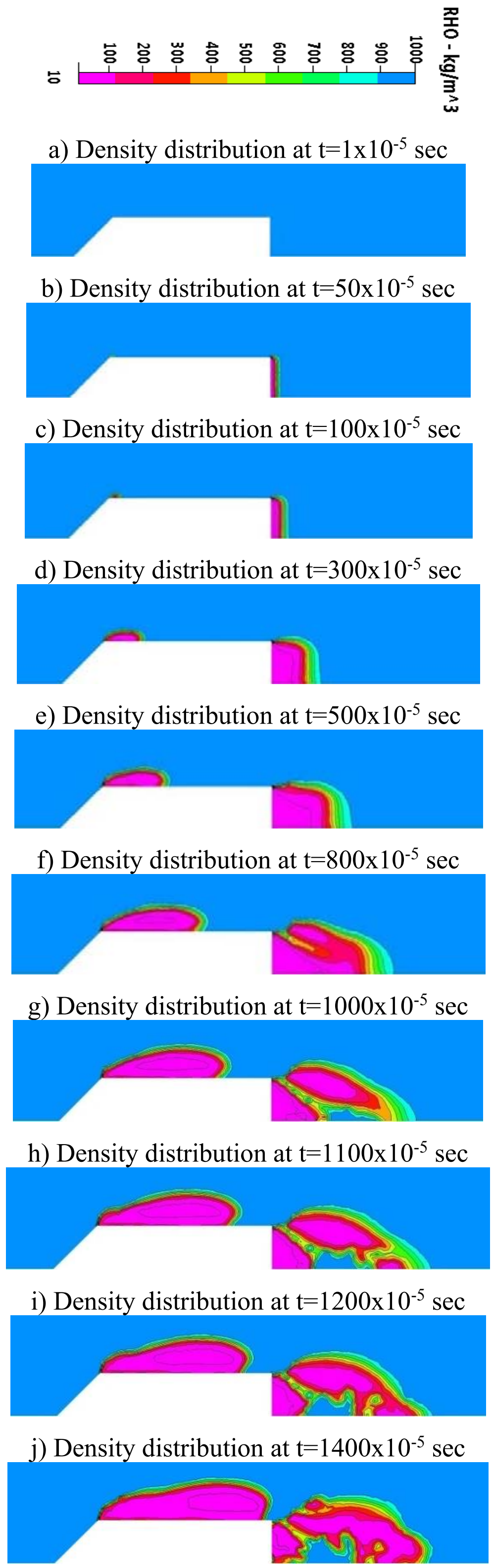

Fig. (12) Supercavitating cavities formation upon conical projectile at speed 60 m/s, using unstructured mesh domain.

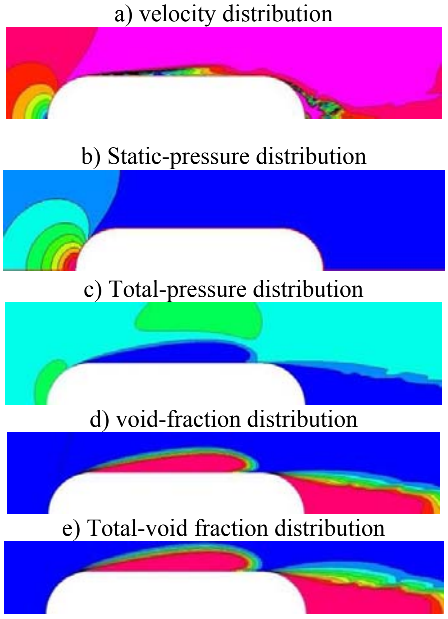

Fig. (13) Flow condition around hemisphere projectile using structured grid at supercavitating condition: σ=0.0555, u= 60 m/s, R_{en}=306 x10^6, and t= 0.014 sec.

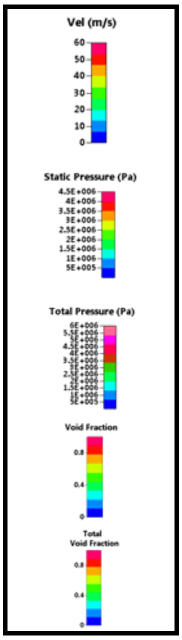

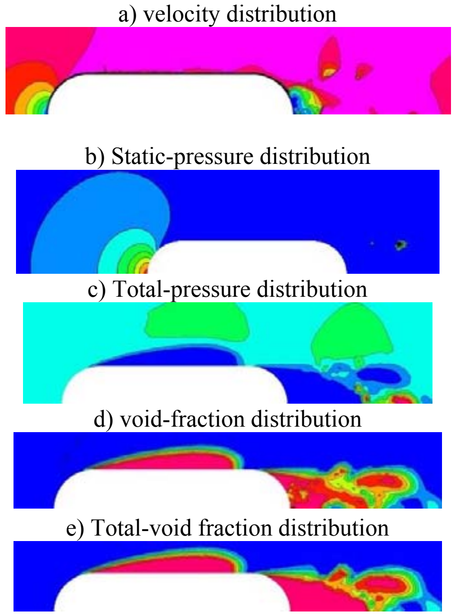

Fig. (14) Flow condition around hemisphere projectile using unstructured grid at supercavitating condition: σ=0.0555, u= 60 m/s, R_{en}=306 x10^6, and t= 0.014 sec.

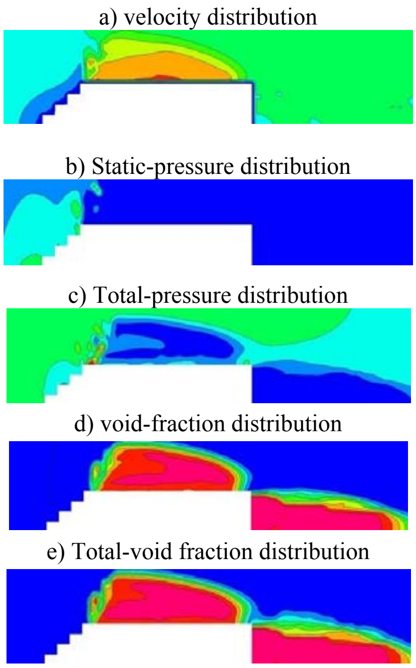

Fig. (15) Flow condition around telescopic projectile using structured grid at supercavitating condition: σ=0.0555, u= 60 m/s, R_{en}=306 x10^6, and t= 0.014 sec.

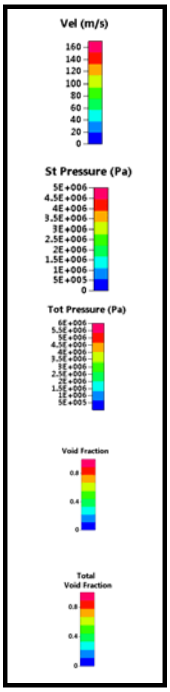

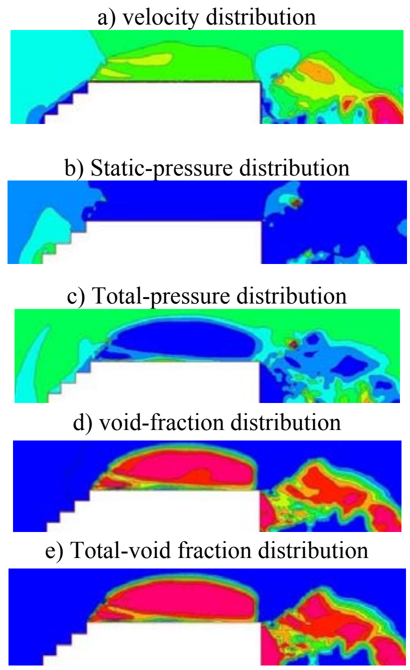

Fig. (16) Flow condition around telescopic projectile using unstructured grid at supercavitating condition: σ=0.0555, u= 60 m/s, R_{en}=306 x10^6, and t= 0.014 sec.

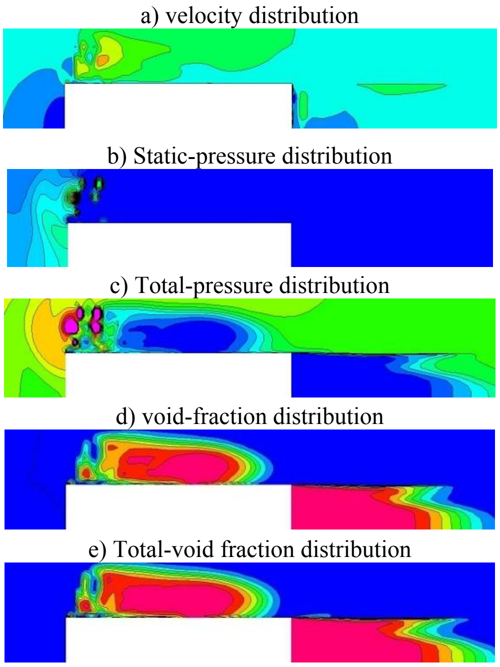

Fig. (17) Flow condition around blunt projectile using structured grid at supercavitating condition: σ=0.0555, u= 60 m/s, R_{en}=306 x10^6, and t= 0.014 sec.

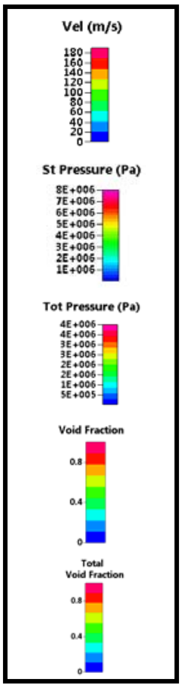

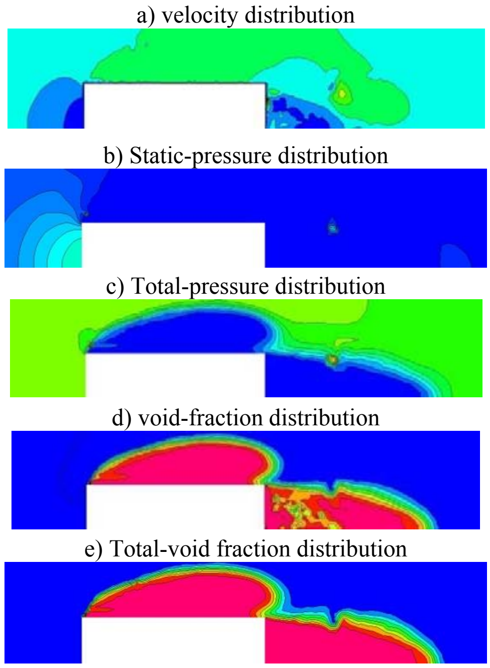

Fig. (18) Flow condition around blunt projectile using unstructured grid at supercavitating condition: σ=0.0555, u= 60 m/s, R_{en}=306 x10^6, and t= 0.014 sec.

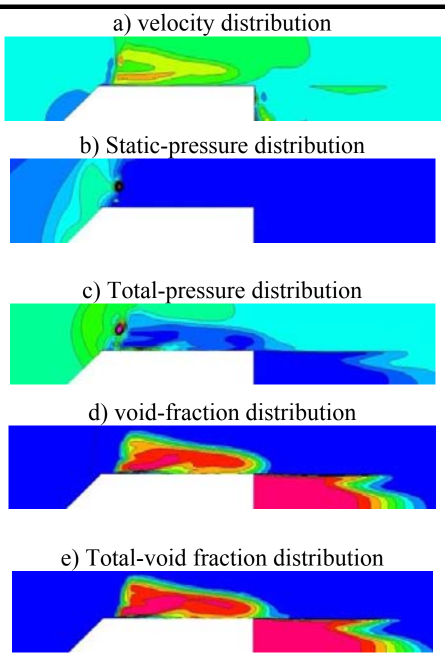

Fig. (19) Flow condition around conical projectile using structured grid at supercavitating condition: σ=0.0555, u= 60 m/s, R_{en}=306 x10^6, and t= 0.014 sec.

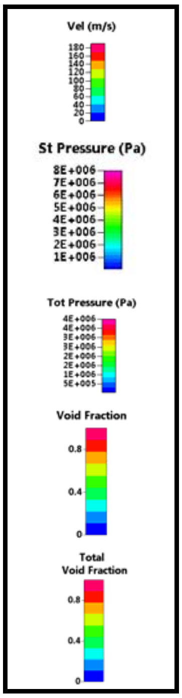

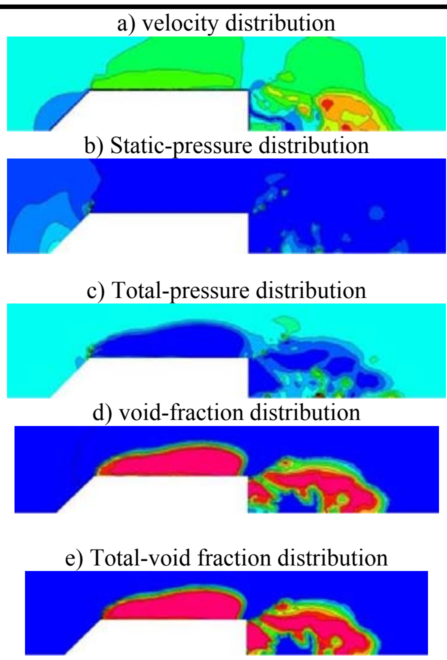

Fig. (20) Flow condition around conical projectile using unstructured grid at supercavitating condition: σ=0.0555, u= 60 m/s, R_{en}=306 x10^6, and t= 0.014 sec.

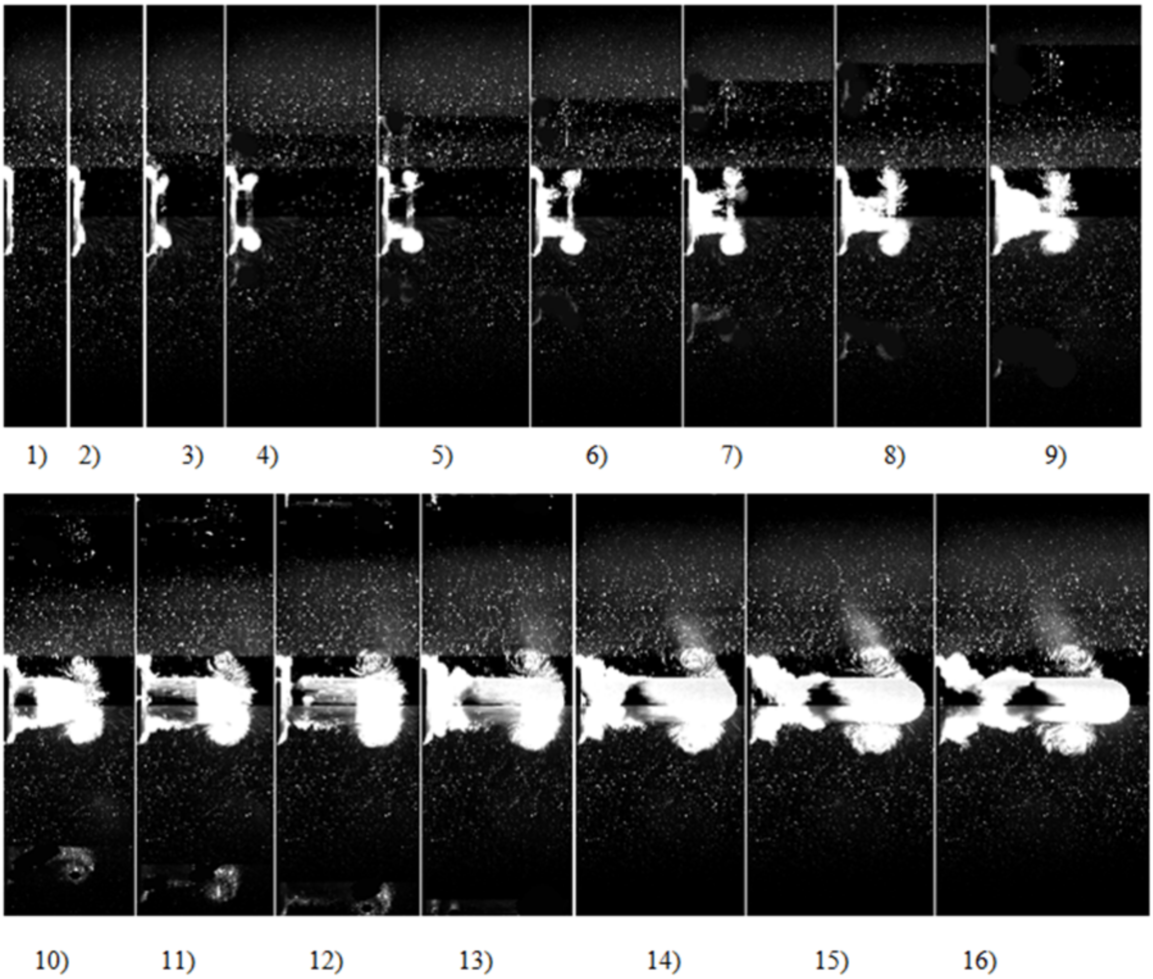

Fig. (21) Formation of cavitating vortex ring,(Mostafa et al. 2001).

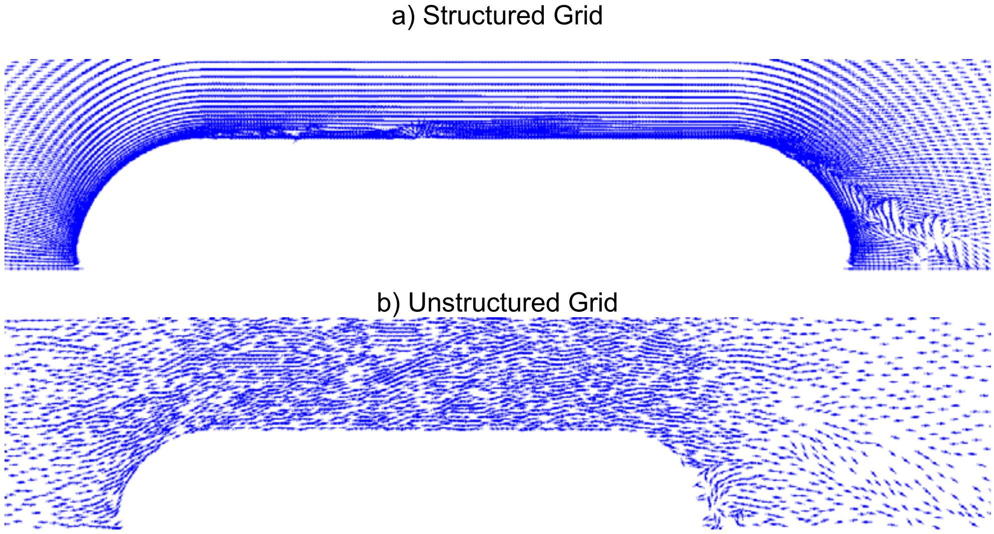

Figure (22) velocity vectors for hemispherical projectile using structured grid at supercavitating condition: σ=0.0555, u= 60 m/s, R_{en}=306 x10^6, and t= 0.014 sec.

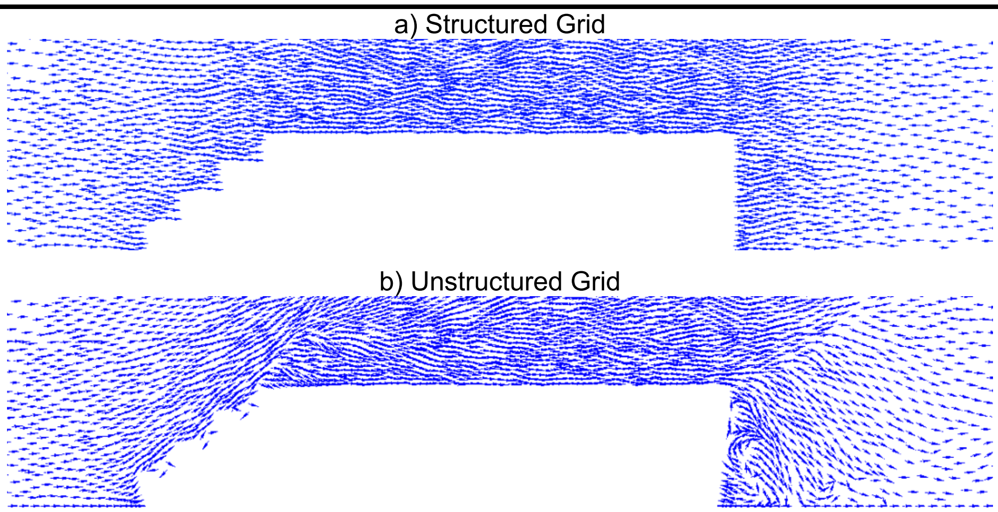

Figure (23) velocity vectors for telescopic projectile using structured grid at supercavitating condition: σ=0.0555, u= 60 m/s, R_{en}=306 x10^6, and t= 0.014 sec.

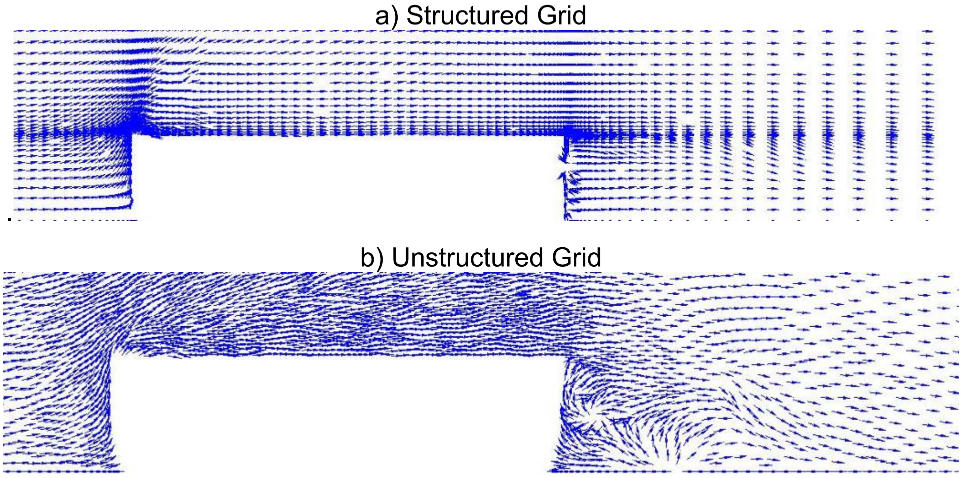

Figure (24) velocity vectors for blunt projectile using structured grid at supercavitating condition: σ=0.0555, u= 60 m/s, R_{en}=306 x10^6, and t= 0.014 sec.

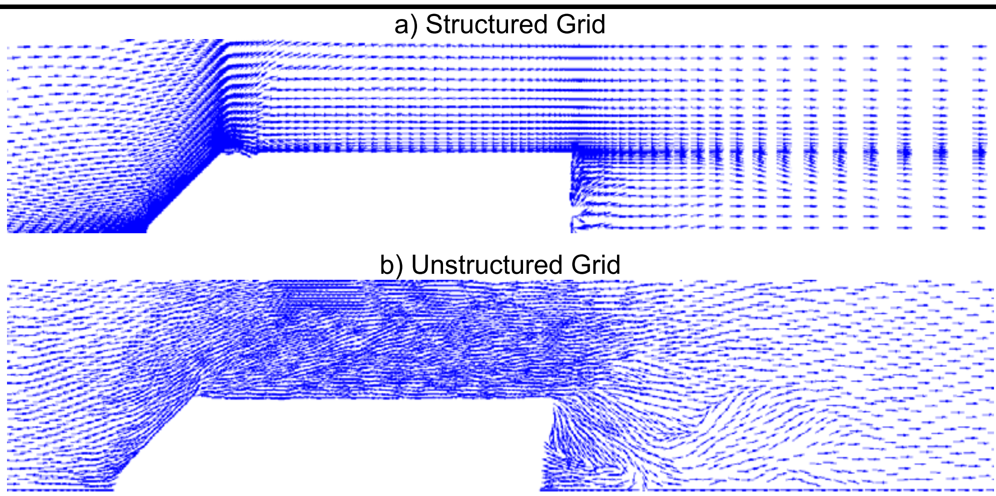

Figure (25) velocity vectors for conical projectile using structured grid at supercavitating condition: σ=0.0555, u= 60 m/s, R_{en}=306 x10^6, and t= 0.014 sec.

REFERENCES:

[1] Ahn, S. Sik, "An Integrated Approach to The Design of Supercavitating Underwater Vehicles" Ph. D. Thesis. Georgia Institute of Tecnology. 2007.

[2] Alyanak, E., Grandhi, R. and Penmetsa R., February "Optimum design of a supercavitating torpedo considering overall size, shape, and structural configuration" Inter. J. of Solids and Structures, Vol. 43, Issues 3–4, pp. 642-657. 2006

[3] ESI-CFD, “CFD-ACE+ Theory and Users’ Manuals”, January, 2010.

[4] Hammitt, F. G., "Cavitation and multiphase flow phenomena" McGraw-Hill International Book Co., New York 1980.

[5] Hinze, J.O., 1975, “Turbulence” McGraw-Hill Book Co., Second Edition.

[6] K. R., November, “Trajectory Optimization Strategies for Supercavitating Vehicles", MSc. Thesis, School of Aerospace Engineering Georgia Institute of Technology, 2005.

[7] Kinnas, S.A., Mishima, S., Brewer, W.H., 1994 "Non-linear analysis of viscous flow around cavitating hydrofoils" Twentieth symposium on naval hydrodynamics, University of California, Santa Barbara, CA.

[8] Mostafa, N. H., Nayfeh, A, Vlachos, P. and Telionis, D., 2001, “Cavitating Flow Over a Projectile” 39 th AIAA Aerospace Science Meeting and Exhibit, 2001-1041, Reno, Nevada, USA.

[9] Mostafa, Nabil H., “Computed Transient Supercavitating Flow Over a Projectile”. The Nine International Conference of Water Technology. Alexandria, Egypt, March, 2005.

[10] Owis, F. M. and Nayfeh, Ali H., " Computations of the Compressible Multiphase Flow Over the Cavitating High-Speed Torpedo" Transactions of the ASME. J. of Fluids Eng· Vol. 125 PP. 459-468, 2003.